communications sustainability

A Nature Portfolio journal

Article

https://doi.org/10.1038/s44458-026-00077-z

Superconducting hybrid energy transmission and storage system and its projected impact on a sustainable energy future

Xiaoyuan Chen[1,2,7], Yu Chen[3,7], Shan Jiang[4], Mingshun Zhang[4], Jinxin Yue[3], Zhihao Chen[3], Chonghao Zhu[3], Siyuan Bao[3], Guozhang Wang[3], Yang Zhan[3], Lin Fu[3,5] ✉ & Boyang Shen[3,5,6] ✉

For the target of 2060 carbon neutrality, extensively increasing the utilisation of solar and wind renewables poses a challenge in surplus energy compensation and multi-site long-distance power transmission. In this article, we proposed a superconducting hybrid-energy transmission and storage system, which can realise surplus energy absorption through large-scale liquid hydrogen production/storage consumption and large-capacity multi-energy transmission. This article uses the real data of renewable power generation and the real data of electricity generation/demand in provinces in China to perform realistic technical and economic analysis. The results show the proposed hybrid-energy system can potentially expand the existing renewable power generation capacity by 2 times and liquid hydrogen production capacity by 4.8 times. Overall, the proposed system can expand the utilisation of renewable energy through the large capacity energy transmission and energy conversion/storage, and solve the electricity generation-consumption imbalance in various regions and realise potential 100% renewable energy demand-fulfilment.

It is estimated that carbon neutrality can be achieved in some countries by 2060 through a high proportion of renewable energy and decarbonisation technologies[1–3]. Renewable energy technologies, in particular solar and wind energy, have achieved rapid technological progress in the recent past[4,5]. Large-scale offshore wind power utilisation has shown great potential in energy transition[6–8]. The global deployment of photovoltaic and wind power has been re-optimised, and tried to minimise the levelised cost of electricity[9]. With the rapid decline in the cost of renewable energy generation, high percentages of renewable or even 100% renewables (using solar + wind power to cover all energy demand in certain areas) are considered as an effective approach to a net-zero carbon energy system in the future[10,11].

However, renewable energy is intermittent, fluctuating, and random[12]. In addition, climate variability influences renewable electricity supply and hence the overall system reliability[13]. The large-scale grid integration with renewable energy poses great challenges to the secure and stable operation of energy systems[13,14]. Energy storage technology is an important method to maintain the stability of the power system[15–17], especially advanced energy storage technologies with large capacity, fast response, and wide time-scale[18–20]. As renewable energy usage increases, there is a need to increase the allocation of transmission infrastructure from renewable energy sources to central load over longer distances[21], and smooth the fluctuation of renewable energy output while keeping proper energy storage[22].

At present, high-voltage direct current (HVDC) transmission system is the primary solutions to address generation-consumption gaps across different regions and long-distance electricity transmission challenges[23]. Cheng et al.[24] proposed an integrated transmission expansion framework that used optimisation and geographic information system (GIS) tools to identify long-distance HVDC routes. Ren et al.[25] showed that ultra-high-voltage transmission in China could significantly increase renewable electricity production and raise the share of electricity in end-use energy consumption. Shufian et al.[26] analysed voltage source converter (VSC) HVDC and control strategies for linking large offshore wind farms to onshore grids, offering technical solutions to enhance stability and accommodate variable renewable generation over long distances. Despite these advantages, HVDC

[1]School of Engineering, Sichuan Normal University, Chengdu, China. [2]Sichuan Energy Internet Research Institute, Tsinghua University, Chengdu, China. [3]College of Transportation, Tongji University, Shanghai, China. [4]College of Electrical Engineering, Sichuan University, Chengdu, China. [5]School of Materials & Energy, Lanzhou University, Lanzhou, China. [6]Department of Engineering, University of Cambridge, Cambridge, United Kingdom. [7]These authors contributed equally: Xiaoyuan Chen, Yu Chen. ✉e-mail: lin.fu.2017@outlook.com; shenboyang1990@outlook.com

systems remain vulnerable to fault currents. Moreover, ultra-high-voltage HVDC deployment is constrained by high converter-station costs, extensive land requirements, the need for advanced control technologies, and strict corridor siting limitations.

Hydrogen (H_2) can be a clean feedstock and also a major energy carrier, and using hydrogen can significantly reduce carbon emissions[27]. Europe considers connecting energy networks through H_2 corridors[28], enabling the coupling of electricity and hydrogen to promote zero carbon[29,30]. However, high-percentage renewable energy generation requires stronger transmission capacity, particularly for multi-site renewable energy sources[31]. Extra long-distance power transmission is an important feature of future renewable energy networks, and there are substantial obstacles such as land acquisition and site selection, project cost sharing, and coordination between regulators, which limit the expansion of extra long-distance renewable energy transmission[32–34].

High-temperature superconducting (HTS) cables have the advantages of virtually zero-loss transmission, large energy transmission capacity and compact configuration for long-distance installation, which is an ideal transmission technology for future renewable energy systems[35]. Combining a superconducting cable with a liquid hydrogen (LH_2) pipeline can offer a unique solution to simultaneously transmit two energies: electricity and hydrogen[36]. In 2013, the hybrid energy transmission of LH_2 and electricity using superconducting cables was experimentally verified at an early stage[37,38]. In recent years, researchers have begun to study the long-distance transmission of hybrid-energy pipelines. A 30 km submarine hybrid-energy pipeline was designed from the offshore plant to the port of Ravenna, transmitting both electricity and LH_2[39]. The European project SCARLET planned to develop onshore and offshore electricity-hydrogen hybrid-energy pipelines at the gigawatt level[40,41]. The conceptual schematic of the cross-Pacific Ocean superconducting hybrid-energy pipeline was preliminarily designed, which has the potential to meet the needs of long-distance and large-scale energy transmission[42].

We have also done upfront work on electricity-hydrogen hybrid-energy pipelines, e.g. the core of the hybrid-energy pipeline (superconducting stacked cables) was experimentally fabricated and measured to verify the high capability of electrical power transmission[43–45], and more complex cable/pipeline structures have been designed[46–48]; the structure design of electricity-hydrogen hybrid-energy pipelines was done, which can transmit 15 MW electricity + 0.7 kg/s hydrogen[49]; the design of electricity-hydrogen hybrid-energy systems to integrate the transportation systems and renewable energy systems[49–51].

The existing literatures of electricity-hydrogen hybrid-energy pipelines mainly focus on the experimental works on short-distance samples, as well as pipeline modelling with technical merit analysis in certain regions. The main contributions of this article are:

(1) This article uses the real data of renewable power generation and the real data of electricity generation/demand. We proposed a superconducting hybrid-energy transmission and storage system to investigate how it can solve the loss problem of simultaneous electricity-hydrogen multi-energy transmission, and how to compensate for the surplus renewable energy.

(2) For the target of 2060 carbon neutrality and potential 100% renewable energy demand-fulfilment, this article shows how the proposed system can enlarge the utilisation of renewable energy regarding the large-capacity energy transmission and energy conversion/storage, and also shorten the electricity generation-consumption gap.

Results

Background and proposed hybrid-energy system

The research object of this article is the current and future energy system of China. The country's area is around 9,600,000 km^2, whose size and geographic diversity are comparable to Europe, and the size and energy feature diversity of each province are also comparable to each European country. The research object reaches a certain level of universal significance.

The article included the real data of wind/solar and other renewable power generation, as well as the real data of the electricity generation and demand of all the provinces in the country. The distribution of the electricity generation-consumption gap in 31 provinces (in the Chinese Mainland) in the first half of 2024 is shown in Fig. 1a. The total electricity consumption in the country was 4,688.45 billion kWh, and the total power generation was 4,219.62 billion kWh[52]. Among them, fossil-fuel power generation accounts for 67% of the total power generation, and wind and solar power generation account for 14.8%. Jiangsu, Zhejiang, Guangdong and other 17 regions consume more electricity than power generation, and require extra inter-provincial power supply. However, Neimenggu had the highest renewable energy generation capacity due to its favourable geographical advantages. Imbalanced energy generation and demand can be clearly seen.

Renewable energy generation (mainly wind and solar power) is estimated to increase up to 600% between 2020 and 2060, and is expected to account for about 80% of total electricity generation[53,54]. By contrast, the fossil-fuel power is projected to fall from over 60% to just 7.5%. However, renewable energy generation is intermittent and fluctuating. Figure 1b presents the total capacities of wind and solar power in 2024 and their projected capacities for 2060. The 2060 values were estimated as six times the wind and solar generation in 2024. The green and red shaded areas indicate the incremental contributions from wind and solar power, respectively.

The electricity generation-consumption gap in 31 provinces in 2024 and 2060 is illustrated in Fig. 1c. With an increasing proportion of renewable energy generation, Neimenggu, Yunnan and Gansu have more surplus energy, but the generation-consumption gap in zones like Shanghai, Jiangsu and Zhejiang is even larger.

Figure 1d, e shows maps of the electricity generation-consumption gap in 31 provinces in 2024 and 2060. Energy-scarce provinces require greater energy supply, while provinces with excess renewable energy require greater energy export capacity. We proposed a superconducting hybrid-energy transmission and storage system, which can use superconducting cables to transmit electricity and hydrogen, and simultaneously compensate surplus renewable energy and store hydrogen energy.

The demand for energy transmission, and the proposed superconducting hybrid-energy transmission routes in 2060 are shown in Fig. 2. The proposed hybrid energy system can transmit energy from the provinces with redundant energy to the provinces with energy shortage, and effectively solve the problem of renewable energy compensation and transmission. Figure 2 shows the geographical schematics of the proposed superconducting hybrid-energy transmission and storage, which needs to be reasonably designed according to the actual energy demand of each region to achieve economic and flexible energy coordination.

Energy storage, transportation, and distribution within and across regions should follow a unified system-planning framework to enhance overall allocation efficiency and operational security. At the intra-urban and regional scale, renewable energy-rich hubs (such as wind and solar-based H_2 production sites) can serve as core nodes, interconnected by a superconducting hybrid-energy pipeline to form multi-node, closed-loop transmission networks. These configurations enable flexible energy redistribution among load centres, provide redundancy, and improve system reliability.

At the inter-city or inter-provincial scale, energy transmission should primarily serve nearby demand, following the principle of local consumption with complementary exchange. Under this approach, surplus energy is transmitted from resource-abundant areas to neighbouring deficit regions, reducing transmission losses while alleviating local supply-demand imbalances.

For cross-regional and long-distance transmission, system design must balance large-scale transmission requirements with geographical, hydrological, ecological and existing infrastructure constraints. Optimising transmission routes and capacity allocation, together with appropriate structural design of a superconducting hybrid-energy pipeline, is essential for establishing an efficient, secure and coordinated interregional energy transmission system.

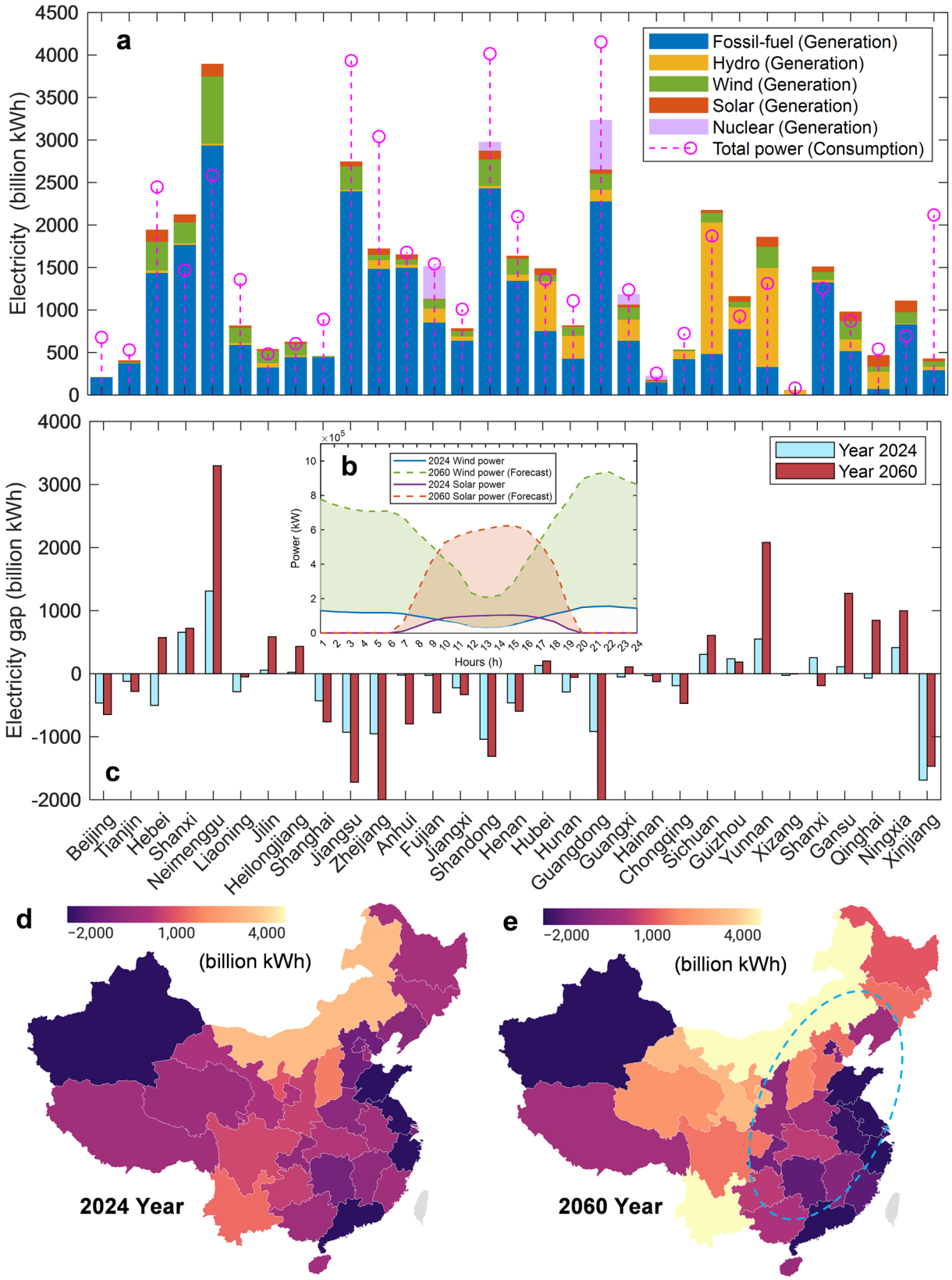

Fig. 1 | Electricity generation/consumption situation in 31 provinces (in the Chinese Mainland). a Electricity generation and consumption in 31 provinces in the first half of 2024. **b** Total capacities of wind and solar power in 2024 and their projected capacities for 2060. **c** Electricity generation-consumption gap in each province in 2024 and 2060. **d** Map of the electricity generation-consumption gap in each province in 2024. **e** Map of the electricity generation-consumption gap in each province in 2060.

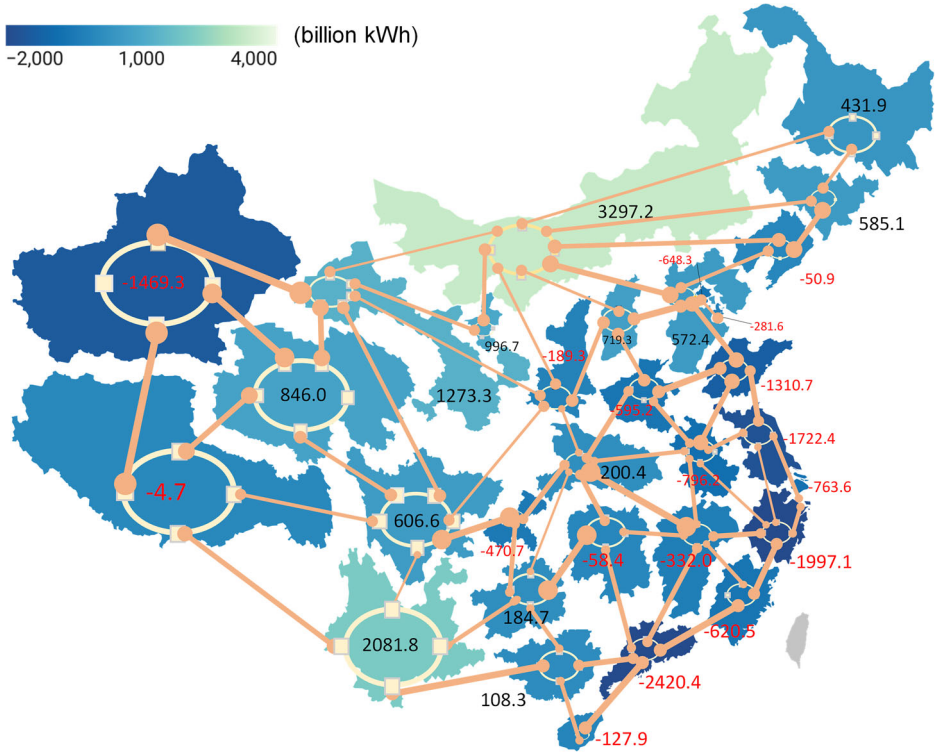

Fig. 2 | Demand for energy transmission, and the proposed superconducting hybrid-energy transmission routes in 2060.

Case study

Chongming Island in China is rich in wind/solar resources, and Fig. 3a shows a schematic of the superconducting hybrid-energy transmission and storage system for the entire region. The red and blue dots represent energy nodes that connect hybrid-energy pipelines and distribute multi-energies to corresponding loads. The renewable energy in the Chongming area will be linked in the form of hybrid-energy pipelines to connect renewable sources and energy nodes, so as to achieve 100% renewable energy generation and utilisation in the region. The part with the red dot connection is used to design and evaluate further.

The design of a superconducting multi-energy storage and transmission system for electricity + hydrogen is illustrated in Fig. 3b. Wind/solar renewable energy is used to generate electricity, and a portion of it is transmitted to sites via superconducting cables. The remaining power is used to produce LH_2 through water electrolysis, and it is stored in LH_2 tanks, and at the same time, LH_2 is used as a cooling medium for HTS cables, realising the integration of electricity/hydrogen transmission and storage. Figure 3c shows the node connections of the entire superconducting hybrid-energy transmission and storage system (corresponding to the part of the red dot connection in Fig. 3a. Assuming that the transmission distance of each node is 10 km, cooling stations are installed at each node to re-cool the LH_2 at the standard operating temperature. Node 1, node 2, node 6 and node 10 need to supply their loads with electricity, 42 MW in total. The LH_2 within this transmission system is 13,800 kg.

Technical analysis of a hybrid-energy pipeline

The typical amount of electricity generated per day, and the amount of electricity that needs to be supplied timely by wind/solar renewables are plotted in Fig. 4a. Among them, the electricity from 1 to 5 and 19 to 24 h is all provided by wind power, and the electricity from 8 to 16 h is all provided by solar power. At 6, 7, 17 and 18 h, 30 MW electricity is provided by wind power and 12 MW by photovoltaic power. The remaining electricity is used to electrolyse water to produce LH_2 for energy storage.

The LH_2 produced by surplus renewable energies is shown in Fig. 4b. Among them, 6656.6 kg of LH_2 is produced by wind power, and 6840.5 kg is by solar power. The total transmission distance is 100 km, the power rate of the superconducting cable is 10 kV/5 kA, and the transmission capacity of LH_2 is 0.16 kg/s. To summarise, the proposed hybrid-energy transmission and storage system can utilise renewable energy with higher capacity and successfully compensate surplus energy, and efficiently transmit electricity-hydrogen hybrid-energy.

For electric energy transmission, superconducting cables can have a maximum current of 10 kA and a maximum transmission capacity of 100 MW, which is twice the existing capacity. For LH_2 transmission, the maximum mass flow rate is 1.4–4.8 times that of the existing one (see Methods section). As shown in Fig. 5a, as renewable energy capacity increases in the future, the capacity of the hybrid-energy pipeline can increase from the grey zone to the green zone. Without additional transmission equipment for electricity and LH_2, larger-capacity and inter-region transmission of multi-energy can be realised.

The conventional transmission of electricity uses an AC 110 kV cable (LGJ-240/30) with an AC resistance of 0.062 Ω/km[46], and a simple calculation of the transmission loss is 2001.7 kW. According to the substation standard, the loss of a 10 kV–110 kV substation system is 158 kW[55]. For a 50 MW case with the distance 100 km, conventional transmission systems have a total loss of 2317.7 kW, while the heat load of the hybrid-energy transmission system is 166.4–199.8 kW and the transmission loss of the proposed system is about 16,640–19,980 kW (factor of 100 at cryogenic temperature 20 K). Figure 5b shows the transmission losses for the 50 MW and the 100 MW cases. In the case of increasing the transmission capacity to 100 MW, the transmission loss of the hybrid-energy pipeline system remains almost unchanged (17,640–20,080 kW), while the conventional transmission loss is 8322.67 kW.

Economic analysis of a hybrid-energy pipeline

This section evaluates the capital expenditure (CAPEX) and operational expenditure (OPEX) of the proposed hybrid-energy pipeline systems to assess their economic benefits. The cost-benefit analysis includes the calculation of indicators such as levelized cost, levelized value, net present value and internal rate of return[56]. The definition of these indicators, as well as the related equations, can be found in a previous publication[57,58].

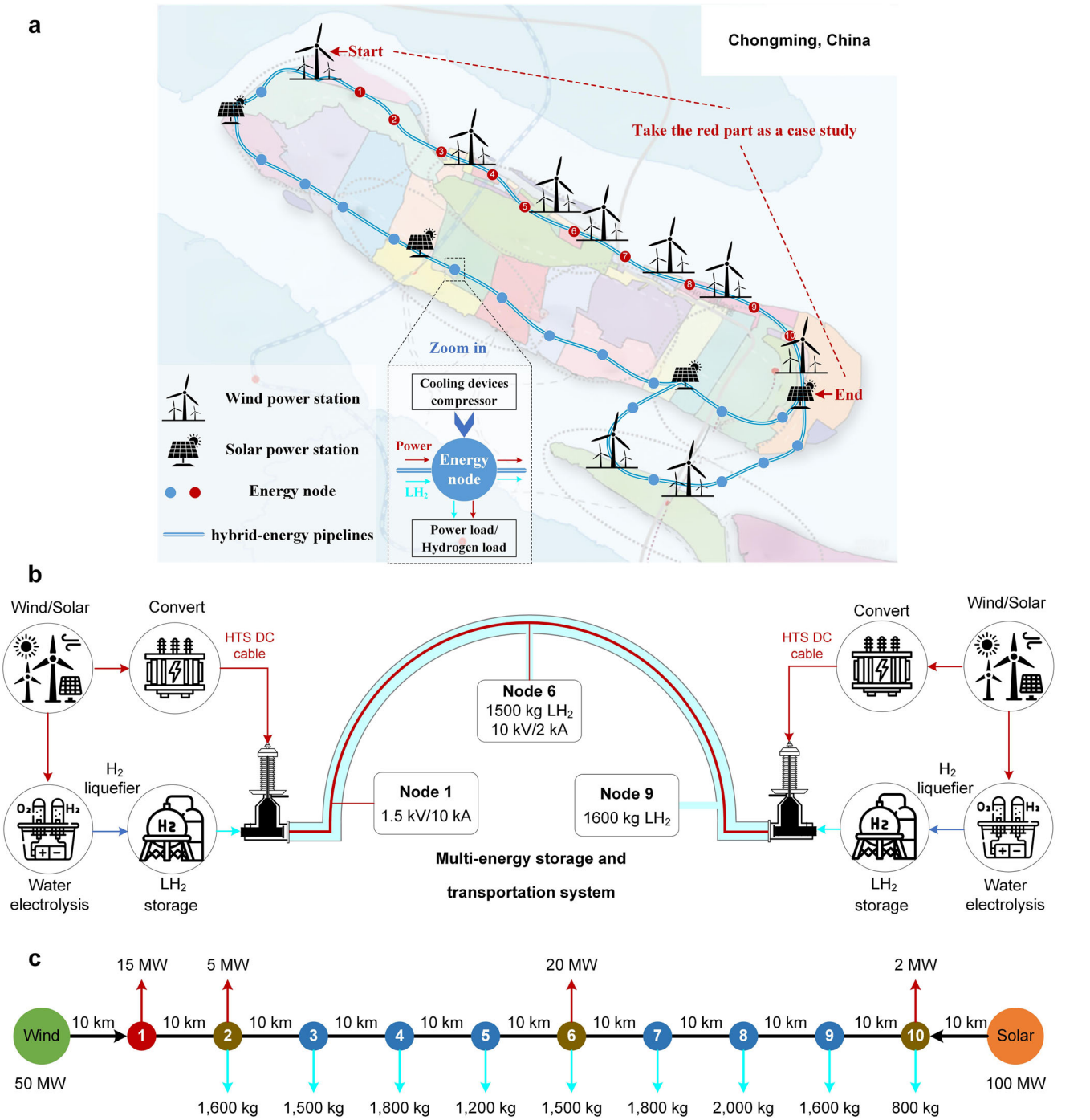

Fig. 3 | Proposed hybrid-energy system and a case study. a Proposed superconducting hybrid-energy transmission and storage system for Chongming, China (the map section was redrawn by the authors with the basic map background by Shanghai Chongming Government, https://www.shcm.gov.cn/bmpd/019001/019001003/20240321/f69f80a9-1dbf-4f45-a037-4c004d6338af.html). **b** Design of superconducting multi-energy storage and transmission system for electricity + hydrogen. **c** Node connections of the entire superconducting hybrid-energy transmission and storage system.

The total levelized cost (TLC) refers to the total cost of the transmission systems, including both the CAPEX and OPEX. The CAPEX occurs at the beginning of the project, while the OPEX is discounted as shown in Eq. (1).

$$TLC = CAPEX + \sum_{k=1}^{n} \frac{OPEX}{(1+i_c)^k} \quad (1)$$

where n is the life of the transmission system (years); k is the calculated value on an annual basis; i_c is the discount rate. CAPEX includes the main components of the proposed hybrid-energy pipeline system (electrolyser system, HTS cables, cryopipes and cooling station) and the values selected for the OPEX are presented in Table 1. The HTS cable structure adopts a configuration with an inner diameter of 0.08 m. Detailed calculations of the copper, electrical insulation, stainless steel, and multi-layer insulation costs were provided in Eqs. (8–15) in the Methods section.

The conventional electricity transmission uses a high-voltage AC cable. Table 2 shows the capital costs and the operating costs of a 110 kV conventional transmission system[59]. At present, hydrogen is mainly transmitted by H_2 trailers, H_2 pipelines and LH_2 tankers.

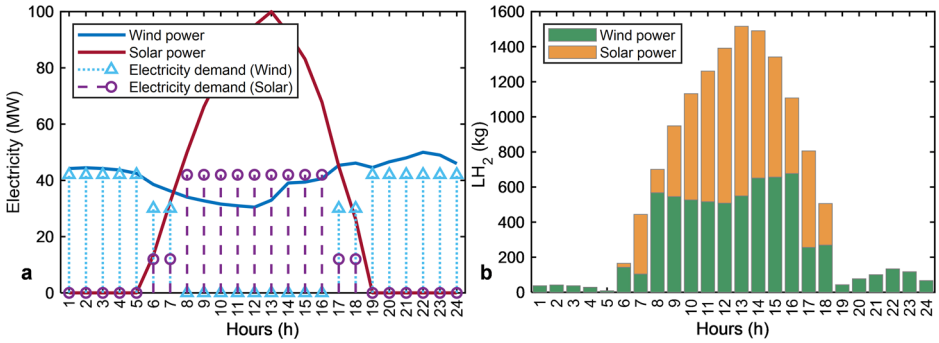

Fig. 4 | Wind/solar energy generation and surplus energy compensation. a Typical amount of electricity generated per day, and the amount of electricity that needs to be supplied timely by wind/solar renewables. **b** LH_2 produced by surplus renewable energies.

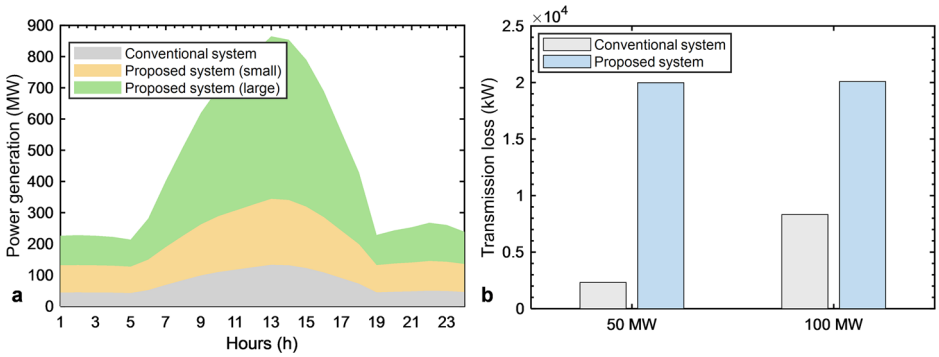

Fig. 5 | Renewable energy generation capacity and transmission loss. a Renewable energy generation by conventional and the proposed system. **b** Transmission losses for 50 and 100 MW cases.

Table 1 | Capital costs and annual operating costs of the proposed hybrid-energy system (10 kA HTS cable and 0.08 mm cryostat inner diameter)

Category	Parameter	Unit cost		Quantity		Cost/M$
H_2 production[80,81]	Electrolyser	4	k$/kW	100	MW	400
	Liquefier	4	k$/kg	13,800	kg	55.2
HTS cable[77]	Copper	5.6	k$/ton	351.68	ton	1.97
	MgB_2 wire	5	$/kA·m	2 × 10 × 100	kA·km	10
	Electrical insulation	10	k$/ton	179.6	ton	1.8
	Cable fabrication*	500	k$/km	100	km	50
Energy pipeline[77]	Stainless steel for cryopipes	5.5	k$/ton	2514.92	ton	13.83
	Multi-layer insulation (25 layers)	27	$/$m^2$	777,150	m^2	20.98
	Pipeline fabrication**	10	k$/km	100	km	1
Cooling station[42]	Cooling cost***	50	M$/unit	10	unit	500
Supporting cost[82]	Labour	1000	k$/km	100	km	100
	Crossing engineering	700	k$/km	100	km	70
	Auxiliary	50	k$/km	100	km	5
Total capital cost (factor of 1.2)						1475.74
Transmission loss and annual operating cost		19,980	kW	0.1	$/kWh	17.5 M$/a

*Cable fabrication costs include structural design cost, material processing cost, labour cost, etc.
**Pipeline fabrication costs include structural design cost, material processing cost, pipeline welding cost, testing cost and labour cost, etc.
***Cooling station has 20,000 W heat load and the RDK-500B Cryocooler Series (40 W@20 K). Considering the construction cost of the cooling station, the equipment cost is about twice.

Table 3 shows the capital costs of four different H_2 transmission systems and the operating costs[60,61]:

a. Conventional cable + H_2 trailer
b. Conventional cable + H_2 pipeline
c. Conventional cable + LH_2 tanker
d. LH_2 superconducting energy pipeline

The costs of energy transmission by the proposed hybrid-energy and conventional systems are shown in Fig. 6. Figure 6a shows the annual investment cost of a 50 MW electricity + 100 MW water electrolysis system and a 100 MW electricity + 500 MW water electrolysis system at a discount rate of 6%. For a small transmission capacity, the investment cost of the proposed hybrid-energy system is approximately two to three times that of the conventional single transmission mode separating electricity and hydrogen. For large transmission capacity, the investment cost of the proposed hybrid-energy system is 1.2 to 1.3 times that of conventional transmission.

Table 2 | Capital costs and annual operating costs of the 110 kV conventional transmission system (50 MW case)

Parameter	Unit cost	Unit	Quantity	Cost / M$
Substation (10 kV/110 kV)[83]	5	M$/unit	2 unit	10
Cable (LGJ-300)[84]	90	k$/km	3 × 100 km	27
Land expropriation and cleaning[84]	165	k$/km	100 km	16.5
Labour[83]	100	k$/km	100 km	10
Total capital cost (factor of 1.5)				95.3
Transmission loss and annual operating cost	2317.7	kW	0.1 $/kWh	2.03 M$/a

Table 3 | Capital costs and annual operating costs of the H_2 production/transmission system (100 MW water electrolysis system)

Parameter	Unit cost		Quantity		Cost / M$
Electrolyser[80]	4	k$/kW	100	MW	400
Liquefier[81]	4	k$/kg	13,800	kg	55.2
H_2 Trailer[85,86]	120	k$/unit	50	unit (280 kg/unit)	6
H_2 transmission (trailer)[87]	1.2	$/kg	13,800	kg/day	6.04 M$/a
Pipeline construction[87]	500	k$/km	100	km	50
H_2 transmission (pipeline)[87]	0.2	$/kg	13,800	kg/day	1.01 M$/a
LH_2 tanker[85,86]	500	k$/unit	4	unit (4000 kg/unit)	2
LH_2 transmission (LH_2 tanker)[87]	2	$/kg	13,800	kg/day	10.1 M$/a

Sensitivity analysis

This section examines the sensitivity of total system investment costs to the variations in electricity price, discount rate, and the costs of key components. Electricity prices are varied in the range of 0.05–0.2 $/kWh, and the discount rate is varied from 0% to 10%. To account for near-term cost uncertainty, the costs of major components (electrolyser, liquefier, MgB_2 wire, and cooling station) are assumed to range between 0.5 and 1.0 times their current baseline values.

Figure 6b illustrates the investment cost of a 100 MW electricity + 500 MW water electrolysis system under discount rates from 0 to 10%. The shaded region indicates the cost envelope, with the upper and lower bounds corresponding to discount rates of 0 and 10%, respectively. As the discount rate increases, the discounted investment cost decreases monotonically. When the discount rate exceeds 3.5%, the proposed hybrid-energy transmission system shows the highest investment cost among the considered configurations. If the discount rate is not considered, the investment cost of the proposed hybrid-energy system gradually becomes lower than that of the single transmission mode.

Figure 6c shows the investment cost of the 100 MW electricity + 500 MW water electrolysis system at a discount rate of 6% under varying electricity prices. The shaded region represents electricity prices ranging from 0.05 to 0.2 $/kWh, corresponding to the lower and upper bounds, respectively. As electricity prices decrease, the cost difference between the hybrid-energy transmission system and conventional transmission progressively narrows. The sensitivity to electricity prices reflects the strong dependence on the generation scale and load-side electricity demand.

In addition to electricity price uncertainty, the investment costs of major system components are expected to decline with increasing market penetration and technological maturation. Figure 6d illustrates the investment costs of the 100 MW electricity + 500 MW water electrolysis system at a discount rate of 6% and an electricity price of 0.1 $/kWh under different equipment cost assumptions. For the proposed hybrid-energy system, the lower bound assumes a 50% reduction in the costs of the electrolyser, liquefier, MgB_2 wire and cooling station, whereas for conventional systems, the lower bound considers a 50% reduction in electrolyser and liquefier costs only. The results indicate that when the initial investment cost of the proposed system falls below 3000 M$, it becomes economically competitive with traditional energy transportation configurations. As future technologies mature, the investment cost of the proposed system is expected to become even more acceptable to the market.

High-capacity energy transmission analysis

As shown in Fig. 5b, at a transmission capacity of 100 MW (110 kV), the conventional transmission system exhibits lower losses than the hybrid-energy transmission system. However, the proposed hybrid-energy transmission system offers greater flexibility for capacity scaling. Owing to the virtually zero resistance of HTS cables, increasing the transmission capacity at a given current rating primarily requires an increase in the electrical insulation thickness. Kim et al.[62] reported that a 220 kV DC HTS cable requires an insulation thickness of approximately 9 mm. Since the voltage level considered in this study is much lower (10 kV), the additional investment cost associated with voltage upscaling can be neglected.

Figure 7a shows the transmission loss of conventional transmission and the proposed hybrid-energy transmission system over a distance of 100 km for different power capacities. The loss calculation methods for the hybrid-energy transmission and conventional systems are given in the Methods section. At transmission capacities below 200 MW, conventional cables exhibit lower losses. At higher power levels, the hybrid-energy transmission system becomes increasingly advantageous. At a transmission capacity of 500 MW, the transmission losses of the conventional transmission and hybrid-energy transmission system are ~50.04 and 20.08 MW, respectively.

Figure 7b further compares the investment costs of the proposed hybrid-energy transmission system and conventional transmission of a 500 MW electricity + 500 MW water electrolysis system at a discount rate 6% and an electricity price of 0.1 $/kWh. The investment cost of the power transmission system is estimated as ten times the baseline values listed in Table 2. The results indicate that the hybrid-energy transmission system achieves the lowest overall transmission cost after 6.5 years.

Impacts on shortening generation-consumption gaps

The analysis above has verified the technical advantages of the proposed hybrid-energy system in a region. If the proposed system is widely used for hybrid-energy transmission and storage in the entire country, the power generation-consumption gap of all provinces in 2060 can be efficiently improved, as shown in Fig. 8a. Two scenarios are defined. Scenario A (light yellow bar): conventional energy system (80% renewable energy); Scenario B (dark green bar): the proposed hybrid-energy system (100% renewable energy, transmission loss reduces 5% of the gap). The proposed hybrid-energy system can increase the capacity of renewable energy consumption and can potentially achieve 100% renewable energy utilisation. On the one hand, it enables some provinces to reduce their dependence on external electricity supply, such as Jiangsu, Zhejiang, Anhui, etc. On the other hand, it enables the redundancy of electricity demand from shortages in some provinces, such as Liaoning, Shandong, Henan, etc.

Maps of the energy transmission demand of each province under two scenarios are illustrated in Fig. 8b, c. The proposed system can effectively shorten the generation-consumption gap and relieve energy demand from inter-provinces transmission. Figure 8b shows the map of the energy transmission demand of each province in 2060 with a conventional energy system, while Fig. 8c shows the map of the energy transmission demand of each province in 2060 with the proposed hybrid-energy system. The proposed system with advanced energy transmission/storage technology is able to alleviate the energy imbalance of all provinces in the country. The

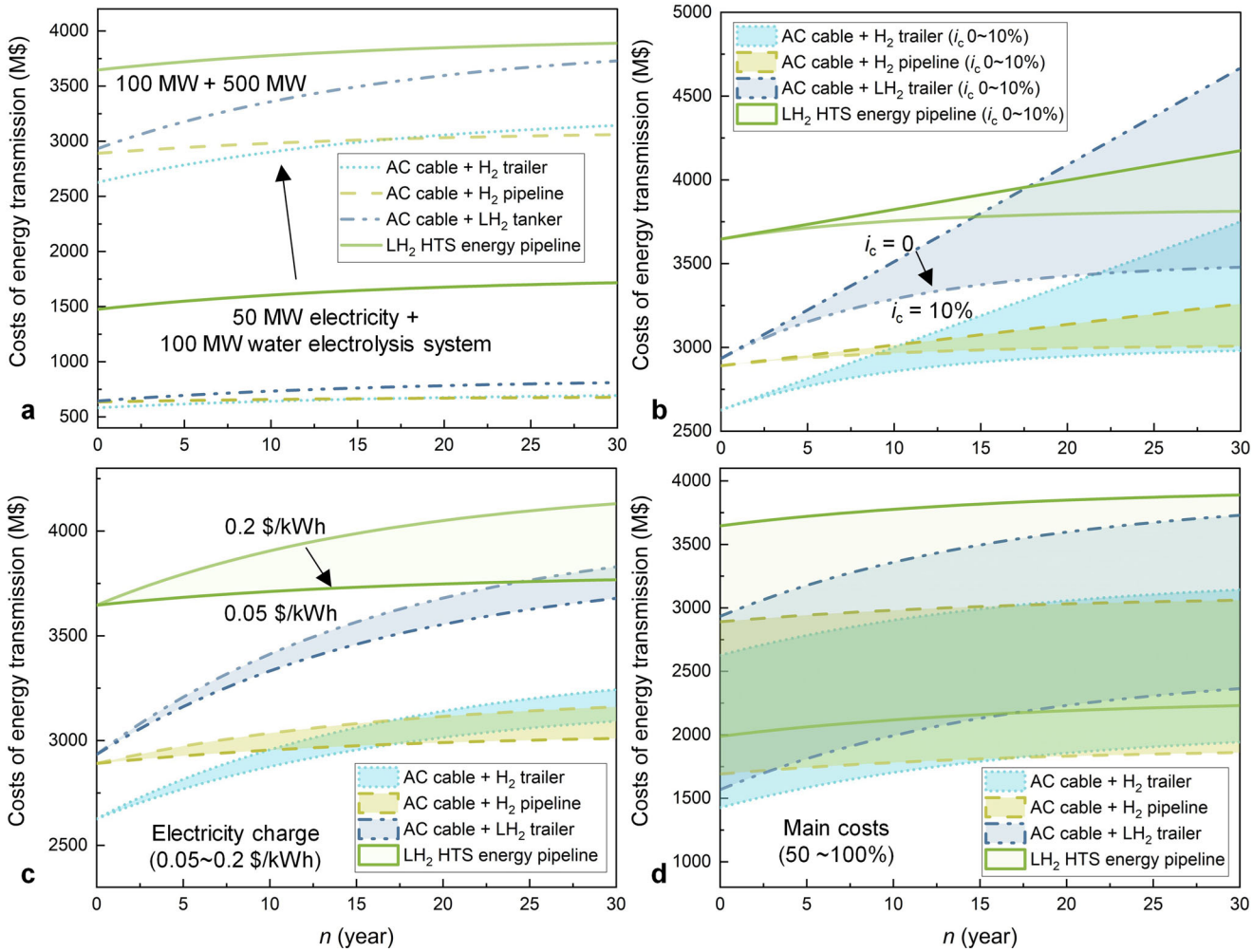

Fig. 6 | Costs of energy transmission: the proposed hybrid-energy system vs the conventional system. a 50 MW electricity + 100 MW water electrolysis system and 100 MW electricity + 500 MW water electrolysis system at a discount rate of 6%. **b** 100 MW electricity + 500 MW water electrolysis system with different discount rates from 0 to 10%%. **c** Investment cost of a 100 MW electricity + 500 MW water electrolysis system at a discount rate of 6% under varying electricity prices. **d** Investment cost of a 100 MW electricity + 500 MW water electrolysis system at a discount rate of 6% and an electricity price of 0.1 $/kWh under different equipment cost assumptions.

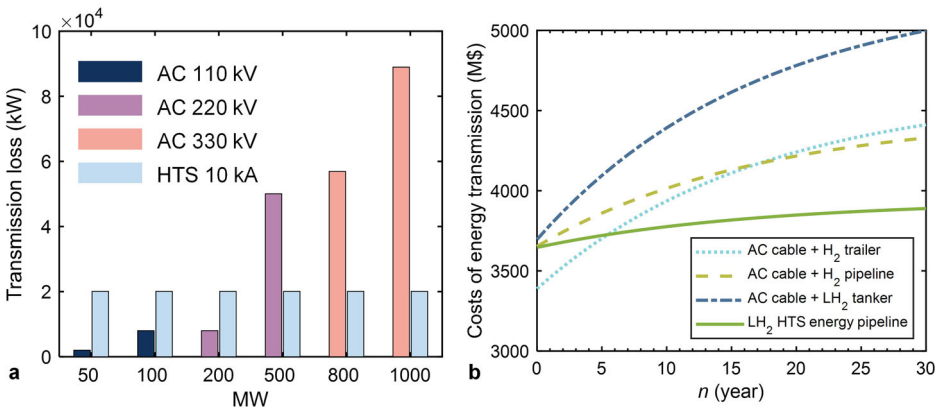

Fig. 7 | Transmission loss and investment cost of different transmission systems. a Transmission loss of conventional transmission and the proposed hybrid-energy transmission system over a distance of 100 km for different power capacities. **b** Investment costs of the proposed hybrid-energy transmission system and conventional transmission of a 500 MW electricity + 500 MW water electrolysis system.

proposed hybrid-energy system can reduce energy shortages in the northern part of the country, particularly the regions near the capital city of Beijing.

The total electricity generation by the conventional energy system and the proposed hybrid-energy system in Shandong Province in 2060 is illustrated in Fig. 8d, and the pink line represents the electricity demand. In the case of carbon neutrality in the future, the proportion of renewable energy power generation will be higher than 80%. However, the generation-consumption gap still cannot be fixed in some high-energy-demand regions such as Shandong and Jiangsu. Future work requires optimisation based on actual energy demand characteristics.

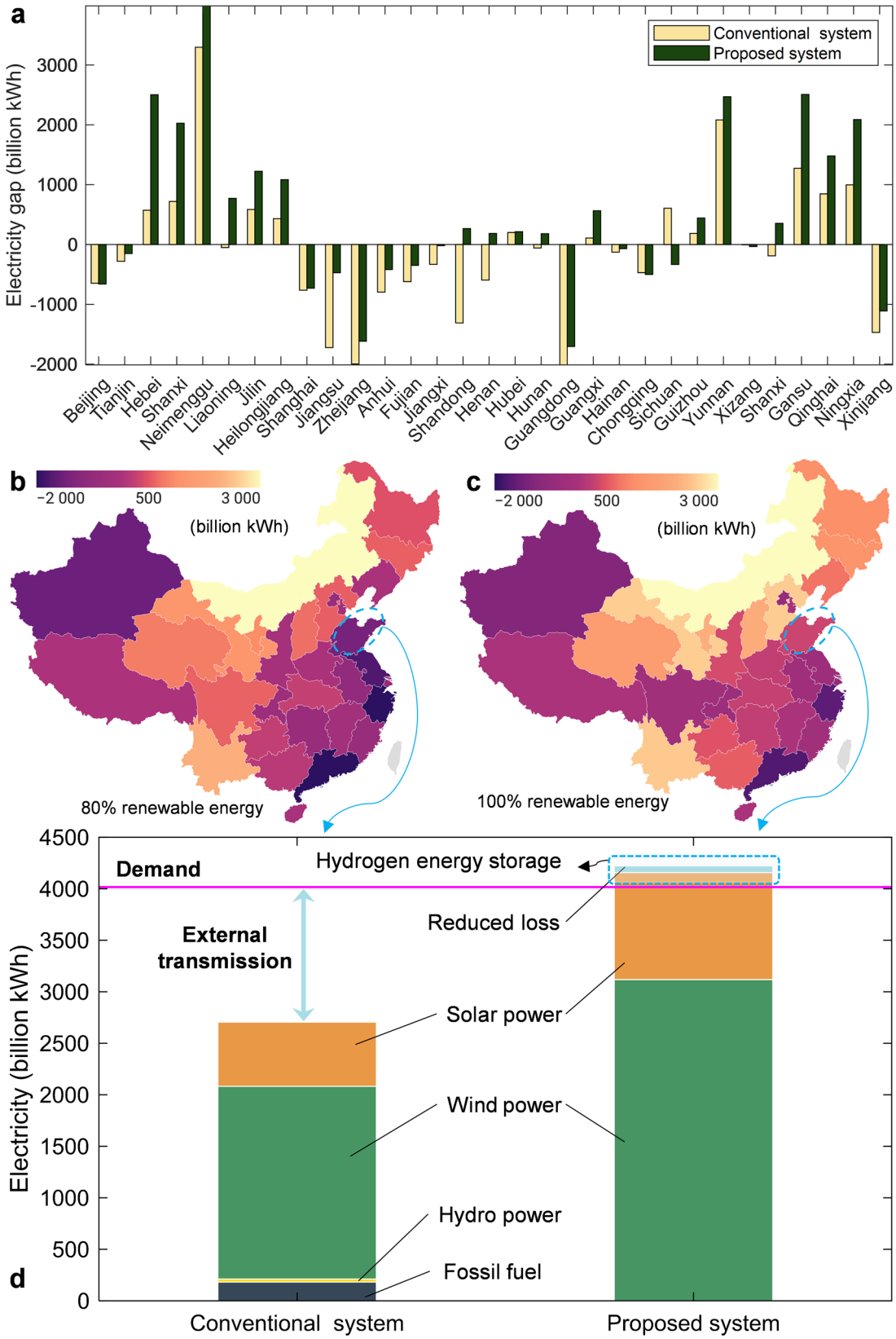

Fig. 8 | Contribution of the proposed hybrid-energy system: shorten the electricity generation-consumption gap and realise potential 100% renewable energy demand-fulfilment. a Power generation-consumption gap of 31 provinces in 2060. **b** Map of the energy transmission demand of each province in 2060 with a conventional energy system. **c** Map of the energy transmission demand of each province in 2060 with the proposed hybrid-energy system. **d** Total electricity generation by the conventional energy system and the proposed hybrid-energy system in Shandong province in 2060.

If the proposed hybrid-energy system is adopted, (1) More renewable energy can be properly utilised for power generation and the electricity generated by renewables can be greater; (2) at the same time, the surplus renewable energy can be used to produce LH_2 for energy storage; (3) the problem of transmission loss can be greatly relieved. Overall, the proposed hybrid-energy system can balance electric energy generation and consumption, and 100% renewable energy generation and energy demand-fulfilment inside the region can potentially be achieved.

Discussion

In the large-scale deployment of the proposed hybrid-energy transmission system, environmental and safety considerations constitute critical design constraints. LH_2 is characterised by an extremely low boiling point (20.3 K) and a wide flammability range, resulting in leakage, dispersion, and ignition behaviours that differ fundamentally from those of conventional energy carriers. In pipeline-based transmission, these risks necessitate the integration of multi-layer sealing architectures, continuous H_2 leak detection, and rapid isolation and venting mechanisms to mitigate fire and explosion hazards associated with the release of cryogenic H_2[63]. Compared with high-pressure H_2 transmission, LH_2 pipeline operates at lower pressures for an equivalent energy throughput, thereby partially alleviating transient risks arising from mechanical failure. However, the cryogenic operating conditions impose more stringent requirements on material toughness and long-term operational sealing reliability, thereby introducing additional limitations for safe and durable system operation[64].

From an environmental perspective, the hybrid-energy transmission system produces negligible direct greenhouse gas emissions during operation. Its overall environmental performance is thus primarily governed by the H_2 production pathway and the energy efficiency of the associated cryogenic cooling system. Large-scale LH_2 production and its supporting infrastructure can impose notable environmental impacts when assessed from a life cycle perspective, primarily due to the high-energy demand, greenhouse gas emissions from upstream energy supply, and resource use for electrolysers, liquefaction units and cryogenic materials. Even for green H_2, the construction and operation of liquefaction plants, storage tanks, and transportation networks contribute to emissions, land use and material-related environmental burdens. Consequently, the environmental benefits of LH_2 also depend on deep decarbonisation of the energy system and proper infrastructure planning[65].

The long-term reliable operation of the proposed hybrid-energy transmission system mainly has three key challenges:

(1) Cryogenic pipeline structure. Efficient thermal isolation and low heat ingress are essential for long-distance cryogenic pipelines, especially when conveying LH_2 over hundreds of kilometres. In such systems, a vacuum jacketed multi-layer insulation (MLI) structure has been adopted[66], where an interstitial high vacuum virtually eliminates convective heat transfer and the multiple reflective layers significantly suppress radiative heat loads, resulting in very low overall thermal conductivity under high vacuum conditions. Beyond direct LH_2 cooling, several studies have proposed indirect cooling architectures to further enhance thermal stability and safety. For example, some designs placed the HTS cable inside a helium-filled containment tube to achieve indirect cooling, with LH_2 flowing in an outer layer[67]. Alternative concepts introduced a liquid nitrogen (LN_2) thermal shield surrounding the LH_2 channel, thereby reducing heat leakage from the external environment[68]. Experimental studies conducted in Russia compared the thermal performance of three cryostat configurations (vacuum insulation, LN_2 shielding, and LH_2 self-boil-off cooling) over segments of ~10 m[38]. The results indicate that active LH_2 evaporation cooling can provide the most effective thermal insulation among the tested approaches.

(2) Real-time monitoring technology. At the operational level, the high degree of integration between LH_2 infrastructure and HTS components necessitates interdisciplinary monitoring and control strategies[69]. These include real-time cryogenic thermal management, H_2 safety surveillance, and continuous diagnostics of the superconducting electrical state. As transmission scales increase, digitalised operational frameworks and predictive maintenance approaches are expected to play a central role in ensuring long-term system stability and reliability.

(3) System reliability and modular design. During long-term operation, unavoidable thermal cycling and load fluctuations impose cumulative stresses on cryogenic structural materials, insulation layers, and vacuum insulation systems. Key reliability challenges include low-temperature fatigue, thermal contraction mismatch between dissimilar materials, and progressive degradation of sealing performance, all of which can limit system lifetime[70]. To enhance fault tolerance and operational resilience, system-level strategies such as redundant refrigeration architectures, segmented isolation, and modular pipeline design are essential to localise failures and prevent cascading impacts.

Overall, the proposed hybrid-energy transmission system offers substantial potential for large-scale, low-loss, and low-carbon energy transportation. However, its engineering feasibility depends not only on technological maturity but also on a range of interrelated factors, including environmental and safety considerations, cryogenic reliability, and long-term operational stability. Strengthening standards and regulatory frameworks for LH_2 production, storage, transportation, and safety is therefore essential to ensure cost-effective and reliable system operation. Future research should advance in a coordinated manner across system integration, safety standards, cryogenic materials, and operational strategies to enable the large-scale deployment of the proposed hybrid-energy transmission system.

Conclusions

This paper proposed a superconducting hybrid-energy storage and transmission system to address regional energy deficits, as increasing penetration of renewable energy was expected to exacerbate regional supply-demand imbalances. We quantified current energy shortfalls across regions and assessed future imbalance trends under high renewable integration. Based on case studies, a structural model of the hybrid-energy pipeline and a comprehensive techno-economic assessment framework were developed. The proposed system was evaluated against conventional methods, including conventional electrical power cable transmission, H_2 transportation by trailers and pipelines, and LH_2 tanker transportation, while accounting for uncertainties in discount rate, electricity price, and major equipment investment costs. The results indicated that for a transmission distance of 100 km, the proposed hybrid-energy transmission system (500 MW electricity + 500 MW hydrogen) demonstrated clear economic advantages over conventional options. However, transmission capacity and distance remain key constraints affecting both economic viability and operational reliability. Under current configurations, the system investment cost remained relatively high. Looking ahead to 2060, the same system configuration would accommodate up to twice the electricity and 4.8 times the hydrogen throughput without additional capital investment, highlighting its strong scalability potential. With continued advancements in LH_2 and HTS cable technologies, as well as supporting infrastructure, the proposed system could provide a viable and flexible solution for managing variability and regional energy deficits in future energy systems with high shares of renewable generation.

Methods

Structural design of the main hybrid-energy pipeline

Upfront work on the proposed hybrid-energy system has already been established, including the modelling and experimental work[43–51]. As shown in Fig. 3c, the capacity and size of the hybrid-energy pipeline need to be redesigned at different nodes, and this paper takes the annular storage and transportation pipelines as an example to carry out the transmission capacity and loss analysis.

Based on the parameters in the case study, the structure of the hybrid-energy pipeline is designed. Figure 9a shows the structure of the hybrid-energy pipeline, which is mainly composed of a superconducting cable, LH_2, and a cryostat. From the inside to the outside, the HTS cable has the copper

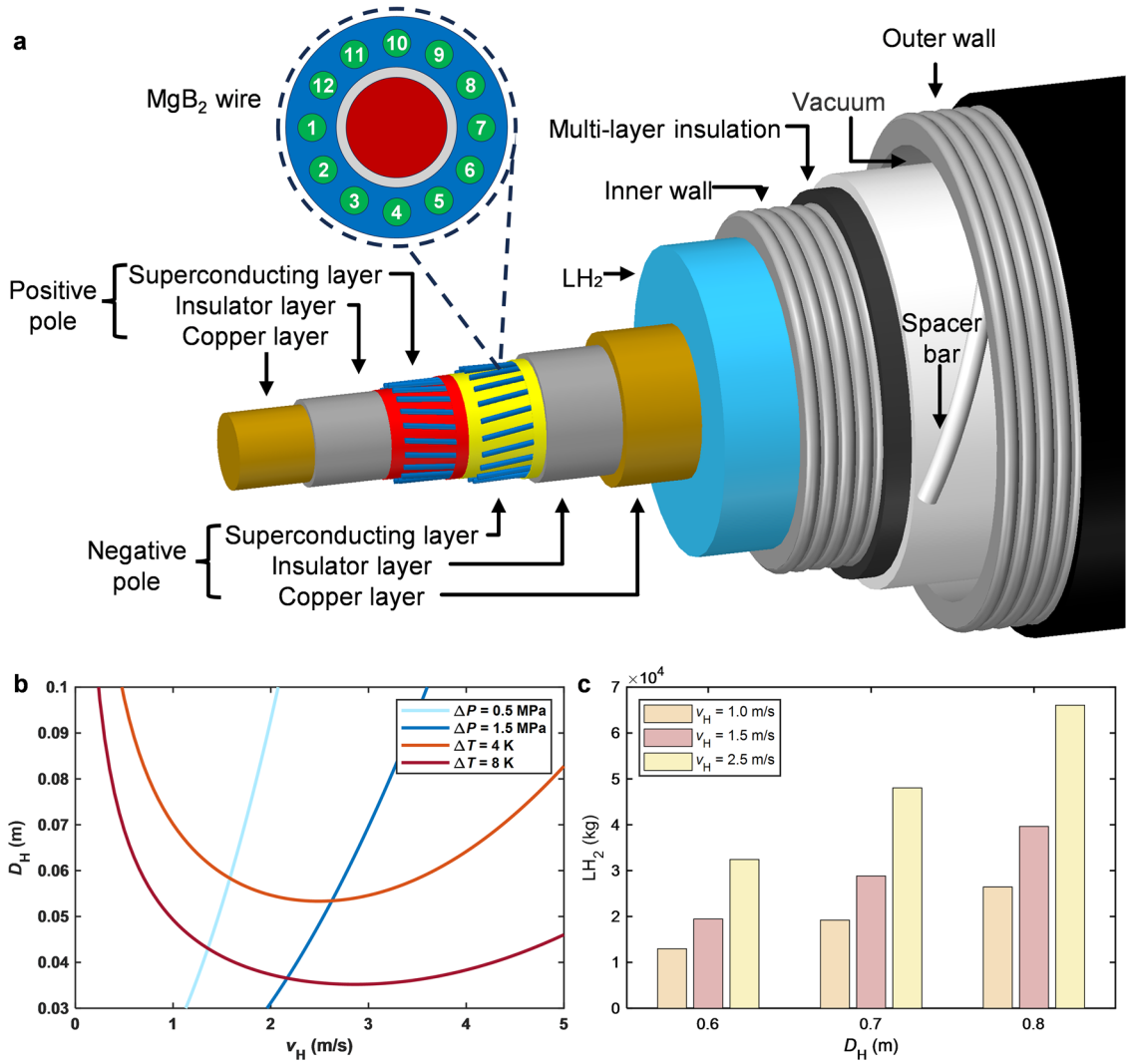

Fig. 9 | Design and analysis of hybrid-energy pipelines. a Structure of the hybrid-energy pipeline. **b** Outer diameter and velocity for a given distance *L* between the cooling stations. **c** Daily capacity of the hybrid-energy transmission with different diameters and flow rates.

layer, the insulating layer and the superconducting layer of the positive and negative electrodes, the insulating layer and the copper layer. From the inside to the outside, the cryostat can be divided into an inner wall, multi-layer vacuum insulation, and an outer wall.

There are several commercial superconducting materials: BSCCO, YBCO and MgB_2 wires[71,72]. MgB_2 superconducting wires have a price advantage over BSCCO and YBCO wires. According to the situation of existing superconducting cable projects, the total cost of the MgB_2 superconducting cable system is much lower than that of the BSCCO or YBCO superconducting cable systems, even when the cooling cost is taken into account. Therefore, considering the cost-effectiveness of superconducting wires in the LH_2 operating temperature region, MgB_2 wires were selected for the proposed system.

Considering the thermal stability, in case the cable is short-circuited occasionally, a copper former should be used to stabilise the transient temperature around the HTS tapes. The minimum cross-sectional area S_{min} of the former copper can be estimated by[49]:

$$S_{min} = \frac{I_\infty \sqrt{t_{eq}}}{\sqrt{\frac{C_{pcu}\rho_{cu}}{\alpha\rho_{rcu}} \ln\left(\frac{1+\alpha(T_s-(T_1-T_H))}{1+\alpha(T_c-(T_1-T_H))}\right)}} \quad (2)$$

where I_∞ is the steady-state fault current; t_{eq} is the equivalent fault time duration; C_{pcu} is the specific heat of copper under a constant pressure, 195 J/kg·K; ρ_{cu} is the copper density, 8960 kg/m^3; α is the temperature coefficient, 0.004 K^{-1}; ρ_{rcu} is the copper resistivity at an initial temperature T_c of 20 K, 0.0395 μΩ·m; T_s is the allowable temperature during the fault, 150 K. T_1 and T_H are the room and LH_2 operating temperatures, respectively. The fault current is three times the rated current, with a fault duration of 1 s. Taking into account the processing margin, the inner diameter of the copper former is 0.015 m.

The schematic of an MgB_2 superconducting cable is shown in Fig. 9a. It consists of a copper core, an iron barrier and 12 twisted filaments immersed in a Monel matrix[73]. The superconducting fraction of the wire is 0.15, and the critical current I_{c0} is about 555 A at 20 K. $J_c(B)$ is the critical current density obtained from the experimental characterisation of MgB_2 wires at 20 K for fields up to 1.7 T[74]:

$$J_c(B) = J_{c0}\left(1-\frac{B}{B_1}\right)\left(1+\frac{B}{B_0}\right)^{-\alpha} \quad (3)$$

where $B_0 = 0.0339$ T, $B_1 = 2.91$ T, $\alpha = 0.232$ and $J_{c0} = 3 \times 10^9$ A/m^2. There are 20 MgB_2 wires in the positive and negative superconducting layers, and the maximum critical current is 13,302 A. The outer diameter of the negative pole superconducting layer is 0.03 m.

The design of the DC HTS cable system is carried out in the following: MgB_2 cable cooled with LH_2. The coolant is introduced at one cooling station at controlled temperature T_{in} and pressure P_{in} and is re-cooled at the

next station after a distance L. The temperature at the outlet section must not exceed a proper limit, T_{max} out, in order to assure appropriate performance of the superconductor. Furthermore, the pressure must not be below a proper limit of P_{min} out in order to avoid the formation of bubbles, and assure appropriate heat exchange conditions as well as appropriate performance of the insulation in case of cold dielectric. The temperature range is 17–25 K, and the pressure range is 0.5–2 MPa.

It is assumed that the pipeline fluid is incompressible, and the cross-section of flow is unchanged. The gradients of pressure and temperature along the length are given by[75]:

$$\begin{cases} \frac{\Delta P}{\Delta X} = \frac{f_H \rho_H v_H^2}{2(D_H - D_0)} \\ \frac{\Delta T}{\Delta X} = \frac{f_H v_H^2}{2(D_H - D_0)C_{pH}} + \frac{4q}{\pi(D_H^2 - D_0^2)\rho_H v_H C_{pH}} \end{cases} \quad (4)$$

where D_H is the outer diameter of LH_2 layer; D_0 is the HTS cable external diameter (inner diameter of LH_2 layer); v_H is the LH_2 average velocity; ρ_H is the LH_2 density; C_{pH} is the specific heat at constant pressure, and f_H is the friction factor.

Equation (4) indicates that two degrees of freedom can be used for regulating the average pressure and temperature gradients in the pipeline: the outer diameter D_H and the velocity v_H of the liquid coolant (the inner diameter is fixed by the electromagnetic design of the cable core). The iso-gradient curves of LH_2 in the D_H-v_H plane are shown in Fig. 9b.

The equation for calculating the mass flow m_H of LH_2 is:

$$m_H = A\rho_H v_H = \frac{\pi}{4}(D_H^2 - D_0^2)\rho_H v_H \quad (5)$$

At present, the daily transmission capacity of LH_2 is 13,800 kg. If the diameter of the LH_2 layer is 0.06 m, the transmission flow rate would be 1.06 m/s calculated by Eq. (5). If the LH_2 diameters are 0.06, 0.07 and 0.08, respectively, the daily transmission capacity of LH_2 at a flow rate of 1.5 m/s would be 19,457, 28,825 and 39,635 kg. At a flow rate of 2.5 m/s, the daily capacity of LH_2 is 32,429, 48,042 and 66,058 kg, respectively.

The daily capacity of the hybrid-energy transmission with different diameters and flow rates is shown in Fig. 9c. Based on the transmission of 13,800 kg per day, the maximum transmission capacity of the 0.06 m diameter at flow rates of 1.5 and 2.5 m/s is 1.4 times and 2.3 times that of the current level, while the maximum transmission capacity at flow rates of 1.5 and 2.5 m/s is 2.9 times and 4.8 times that of the 0.08 m diameter case. With a high proportion of renewable energy in the future, the proposed hybrid-energy system can fully utilise renewable energy, achieving local surplus energy compensation and long-distance transmission.

The heat leakage Q_{cry} of the LH_2 cryostat is given by[76]:

$$Q_{cry} = \frac{2\pi\lambda(T_H - T_l)}{\ln(D_3/D_2)} \quad (6)$$

where D_3 and D_2 are the inner diameter of outer wall and outer diameter of inner wall of the LH_2 cryostat; λ is the equivalent heat conductivity of the multi-layer thermal insulation. The heat insulation materials use 25-μm aluminised mylar and 60-μm glass fabric. If the overall thickness is 10 mm, the heat leakage is 1.564 W/m with the inner diameter 0.06 m of the LH_2 cryostat.

The total heat load of the hybrid-energy pipeline is mainly composed of heat leakage from cryostats and heat leakage at the terminal heat of current leads, ignoring the friction of LH_2 flow[77–79].

$$Q_{total} = Q_{cry} + Q_{lead} \quad (7)$$

where Q_{lead} is the heat leakage of HTS current leads. The heat load of the terminal current lead is 50 W/kA. There are positive and negative leads, and each lead has two terminals, so there is a total of four terminals, and the total heat load is 1000 W (5 kA). Table 4 shows the total heat load of the proposed hybrid-energy pipeline with different inner diameters of the cryostat.

Table 4 | Total heat load of the proposed hybrid-energy pipeline with different inner diameters of the cryostat

Parameter	Value 1	Value 2	Value 3
Cryostat inner diameter D_1	0.060 m	0.070 m	0.080 m
Cryostat inner wall outer diameter D_2	0.068 m	0.078 m	0.089 m
Cryostat outer wall inner diameter D_3	0.088 m	0.098 m	0.109 m
Cryostat outer diameter D_4	0.098 m	0.109 m	0.120 m
Cryostat heat leakage	1.564 W/m	1.735 W/m	1.898 W/m
Current lead heat leakage	1000 W	1000 W	1000 W
Total heat load of a 10 km hybrid-energy pipeline system	16,640 W	18,350 W	19,980 W

Table 5 | Outer diameter of each layer of HTS cable

Parameter	Value
Outer diameter of positive copper layer D_{01}	0.015 m
Outer diameter of positive electrical insulation layer D_{02}	0.017 m
Outer diameter of positive MgB_2 layer D_{03}	0.020 m
Outer diameter of negative MgB_2 layer D_{04}	0.023 m
Outer diameter of negative electrical insulation layer D_{05}	0.025 m
Outer diameter of negative copper layer D_0	0.03 mm

Method for cost calculation of each layer of HTS cable and pipeline

The material costs of the superconducting cable and the pipeline reported in Table 1 were calculated using Eqs. (8–15). Among these, the copper cost of the HTS cable, C_{copper} ($), was calculated as follows:

$$C_{copper} = W_c(\rho_{cu} V_{cu}/1000) \quad (8)$$

$$V_{cu} = L\pi\left(\left(\frac{D_{01}}{2}\right)^2 + \left(\left(\frac{D_0}{2}\right)^2 - \left(\frac{D_{05}}{2}\right)^2\right)\right) \quad (9)$$

where the W_c is the unit cost of copper (5.6 k$/ton); V_{cu} is the volume of copper layer; L is the transmission distance of the hybrid-energy system; D_{01}, D_{05} and D_0 are the diameter of copper layer, as listed in Table 5.

The electrical insulation cost of the HTS cable was calculated as follows:

$$C_{ele} = W_{ele}(\rho_{ele} V_{ele}/1000) \quad (10)$$

$$V_{ele} = L\pi\left(\left(\left(\frac{D_{02}}{2}\right)^2 - \left(\frac{D_{01}}{2}\right)^2\right) + \left(\left(\frac{D_{05}}{2}\right)^2 - \left(\frac{D_{04}}{2}\right)^2\right)\right) \quad (11)$$

where the W_{ele} is the unit cost of electrical insulation (10 k$/ton); ρ_{ele} is the density of electrical insulation material; V_{ele} is the volume of electrical insulation layer.

The stainless steel cost of the cryogenic pipeline was calculated as follows:

$$C_{steel} = W_{steel}(\rho_{steel} V_{steel}/1000) \quad (12)$$

$$V_{steel} = L\pi\left(\left(\left(\frac{D_2}{2}\right)^2 - \left(\frac{D_1}{2}\right)^2\right) + \left(\left(\frac{D_4}{2}\right)^2 - \left(\frac{D_3}{2}\right)^2\right)\right) \quad (13)$$

where the W_{steel} is the unit cost of stainless steel (5.5 k$/ton); ρ_{steel} is the density of stainless steel; V_{steel} is the volume of stainless steel used in the cryogenic pipeline.

The multi-layer insulation (MLI) cost of the cryogenic pipeline was calculated as follows:

$$C_{MLI} = W_{MLI} S_{MLI} \tag{14}$$

$$S_{MLI} = 25 \times L\pi\left(0.5\left(D_3 + D_2\right)\right) \tag{15}$$

where the W_{MLI} is the unit cost of multi-layer insulation (27 $/m^2); S_{MLI} is the total area of multi-layer insulation.

Conventional cable transmission loss

The transmission loss of the conventional AC cable was calculated as follows:

$$P_{ac\_loss} = 3I_{ac}^2 R_{ac} L \tag{16}$$

where R_{ac} is the equivalent AC resistance; I_{ac} is operating current of the conventional AC cable, which was calculated as:

$$I_{ac} = \frac{P_{ac}}{\sqrt{3} U \cos\varphi} \tag{17}$$

where P_{ac} is the transmitted power; U is the voltage rating of the AC cable; cosφ is the power factor, taken as 0.8.

Data availability

The data that support the findings of this study are openly available in [Zenodo] at https://doi.org/10.5281/zenodo.19497133.

Received: 3 November 2025; Accepted: 13 April 2026;
Published online: 11 May 2026

References

1. Davis, S. J. et al. Net-zero emissions energy systems. *Science* **360**, eaas9793 (2018).
2. Chen, X. et al. Pathway toward carbon-neutral electrical systems in China by mid-century with negative CO_2 abatement costs informed by high-resolution modeling. *Joule* **5**, 2715–2741 (2021).
3. Yu, B. et al. Approaching national climate targets in China considering the challenge of regional inequality. *Nat. Commun.* **14**, 8342 (2023).
4. Haegel, N. M. et al. Terawatt-scale photovoltaics: transform global energy. *Science* **364**, 836–838 (2019).
5. van Greevenbroek, K., Grochowicz, A., Zeyringer, M. & Benth, F. E. Trading off regional and overall energy system design flexibility in the net-zero transition. *Nat. Sustain.* **8**, 629–641 (2025).
6. Robertson, A. et al. Considerations for the global commercialization of floating offshore wind energy. *Nat. Rev. Clean. Technol.* **1**, 16 (2025).
7. Pryor, S. C., Barthelmie, R. J. & Shepherd, T. J. Wind power production from very large offshore wind farms. *Joule* **5**, 2663–2686 (2021).
8. Gonzalez, N. et al. Offshore wind and wave energy can reduce total installed capacity required in zero-emissions grids. *Nat. Commun.* **15**, 6826 (2024).
9. Duan, H. et al. Assessing China's efforts to pursue the 1.5°C warming limit. *Science* **372**, 378–385 (2021).
10. Zhu, Z. et al. Designing the future electricity spot market with high renewables via reliable simulations. *Nat. Rev. Electr. Eng.* **2**, 320–337 (2025).
11. Hansen, K., Breyer, C. & Lund, H. Status and perspectives on 100% renewable energy systems. *Energy* **175**, 471–480 (2019).
12. Wang, J. et al. Inherent spatiotemporal uncertainty of renewable power in China. *Nat. Commun.* **14**, 5379 (2023).
13. Zhao, J., Li, F., & Zhang, Q. Impacts of renewable energy resources on the weather vulnerability of power systems. *Nat. Energy* **9**, 1407–1414 (2024).
14. Yu, Y., Liu, G. P., Huang, Y., Chung, C. Y. & Li, Y. Z. A blockchain consensus mechanism for real-time regulation of renewable energy power systems. *Nat. Commun.* **15**, 10620 (2024).
15. Sterl, S. et al. Smart renewable electricity portfolios in West Africa. *Nat. Sustain.* **3**, 710–719 (2020).
16. Fu, L. et al. Hydrogen-electricity hybrid-energy system with superconducting-battery energy storage for urban rail transit: design, case study, and techno-economic analysis. *Appl. Energy* **405**, 127198 (2026).
17. Dowling, J. A. et al. Role of long-duration energy storage in variable renewable electricity systems. *Joule* **4**, 1907–1928 (2020).
18. Yang, W. et al. Pumped storage hydropower operation for supporting clean energy systems. *Nat. Rev. Clean. Technol.* **1**, 454–473 (2025).
19. Kittner, N., Lill, F. & Kammen, D. M. Energy storage deployment and innovation for the clean energy transition. *Nat. Energy* **2**, 17125 (2017).
20. Zhao, A. P. et al. Hydrogen as the nexus of future sustainable transport and energy systems. *Nat. Rev. Electr. Eng.* **2**, 447–466 (2025).
21. Bertsch, V., Hall, M., Weinhardt, C. & Fichtner, W. Public acceptance and preferences related to renewable energy and grid expansion policy: empirical insights for Germany. *Energy* **114**, 465–477 (2016).
22. Li, X., Hui, D. & Lai, X. Battery energy storage station (BESS)-based smoothing control of photovoltaic (PV) and wind power generation fluctuations. *IEEE Trans. Sustain. Energy* **4**, 464–473 (2013).
23. Wang, M. et al. Review and outlook of HVDC grids as backbone of transmission system. *CSEE J. Power Energy Syst.* **7**, 797–810 (2020).
24. Cheng, C. et al. An integrated framework for systematically identifying optimal high-voltage transmission routes in renewable energy systems. *Appl. Energy* **402**, 126908 (2026).
25. Ren, S., Bao, R. & Gao, Z. Arrival of distant power: the impact of ultra-high voltage transmission projects on energy structure in China. *Energy* **316**, 134527 (2025).
26. Shufian, A., Hossain, M. I., Anonto, H. Z. & Rohan, A. I. Enhancing stability in renewable energy transmission using multi-terminal HVDC systems with grid-forming controls for offshore and onshore wind integration. *Sci. Rep.* **15**, 42028 (2025).
27. Yang, X., Nielsen, C. P., Song, S. & McElroy, M. B. Breaking the hard-to-abate bottleneck in China's path to carbon neutrality with clean hydrogen. *Nat. Energy* **7**, 955–965 (2022).
28. Kountouris, I. et al. A unified European hydrogen infrastructure planning to support the rapid scale-up of hydrogen production. *Nat. Commun.* **15**, 5517 (2024).
29. Gils, H. C., Gardian, H. & Schmugge, J. Interaction of hydrogen infrastructures with other sector coupling options towards a zero-emission energy system in Germany. *Renew. Energy* **180**, 140–156 (2021).
30. van der Zwaan, B. et al. Electricity-and hydrogen-driven energy system sector-coupling in net-zero CO_2 emission pathways. *Nat. Commun.* **16**, 1368 (2025).
31. Zhou, Y. & He, J. Development of environmentally friendly high-capacity power cables. *Nat. Rev. Electr. Eng.* **1**, 565–566 (2024).
32. DeSantis, D., James, B. D., Houchins, C., Saur, G. & Lyubovsky, M. Cost of long-distance energy transmission by different carriers. *IScience* **24**, 103495 (2021).
33. Zhuo, Z. et al. Cost increase in the electricity supply to achieve carbon neutrality in China. *Nat. Commun.* **13**, 3172 (2022).
34. Wei, W. et al. Embodied greenhouse gas emissions from building China's large-scale power transmission infrastructure. *Nat. Sustain.* **4**, 739–747 (2021).
35. Coombs, T. A. et al. High-temperature superconductors and their large-scale applications. *Nat. Rev. Electr. Eng.* **1**, 788–801 (2024).

36. Grant, P. M. The supercable: dual delivery of hydrogen and electric power. In *IEEE PES Power Systems Conference and Exposition* 1745–1749 (IEEE, 2004).
37. Vysotsky, V. S. et al. Hybrid energy transfer line with liquid hydrogen and superconducting MgB_2 cable—first experimental proof of concept. *IEEE Trans. Appl. Supercond.* **23**, 5400906 (2013).
38. Kostyuk, V. V. et al. Cryogenic design and test results of 30-m flexible hybrid energy transfer line with liquid hydrogen and superconducting MgB_2 cable. *Cryogenics* **66**, 34–42 (2015).
39. Bracco, M. et al. Design of a submarine 30-km MgB_2 cable for the combined transfer of 0.3 GW e and LH_2 from offshore plants to the Ravenna Port. *IEEE Trans. Appl. Supercond.* **35**, 5400906 (2025).
40. Bruzek, C. E. et al. MgB_2-based MVDC superconducting power cable in liquid hydrogen for hybrid energy distribution. *IEEE Trans. Appl. Supercond.* **34**, 6200405 (2024).
41. Magnusson, N. et al. SCARLET–a European effort to develop HTS and MgB_2 based MVDC cables. *IEEE Trans. Appl. Supercond.* **34**, 5400205 (2023).
42. Qin, B. et al. Liquid hydrogen superconducting transmission based super energy pipeline for Pacific Rim in the context of global energy sustainable development. *Int. J. Hydrog. Energy* **56**, 1391–1396 (2024).
43. Chen, Y. et al. Ultra-low electrical loss superconducting cables for railway transportation: Technical, economic, and environmental analysis. *J. Clean. Prod.* **445**, 141310 (2024).
44. Chen, Y. et al. at al. Current characteristics of stacked HTS conductors with gap optimization: experiment and modeling. *IEEE Trans. Appl. Supercond.* **34**, 4804305 (2024).
45. Chen, Y., Fu, L., Chen, X., Xu, J. & Shen, B. High-current stacked HTS conductors with non-uniform gaps: critical current, AC loss, and fault tolerance. *J. Supercond. Nov. Magn.* **37**, 677–692 (2024).
46. Chen, X. et al. Energy-saving superconducting power delivery from renewable energy source to a 100-MW-class data center. *Appl. Energy* **310**, 118602 (2022).
47. Zheng, Z. et al. Hybrid energy transmission for liquefied shale gas and electricity using cryogenic and superconducting technologies: a technical and economic study of Sichuan. *China Fuel* **333**, 126333 (2023).
48. Chen, X. et al. A 10 MW class data center with ultra-dense high-efficiency energy distribution: design and economic evaluation of superconducting DC busbar networks. *Energy* **250**, 123820 (2022).
49. Fu, L., Chen, X., Chen, Y., Jiang, S. & Shen, B. Hydrogen-electricity hybrid energy pipelines for railway transportation: design and economic evaluation. *Int. J. Hydrog. Energy* **61**, 251–264 (2024).
50. Chen, Y., Chen, X., Fu, L., Jiang, S. & Shen, B. Superconducting hydrogen-electricity multi-energy system for transportation hubs: modeling, technical study and economic-environmental assessment. *Appl. Energy* **401**, 126823 (2025).
51. Wang, G. et al. Low-carbon hydrogen-electricity energy supply networks for China-Thailand international high-speed railway. *Energy* **344**, 139940 (2026).
52. National Energy Administration (NEA). https://www.nea.gov.cn/2024-07/31/c_1310783380.htm (2024).
53. Yang, X. J., Hu, H., Tan, T. & Li, J. China's renewable energy goals by 2050. *Environ. Dev.* **20**, 83–90 (2016).
54. Chandler, W., Chen, S., Gwin, H., Lin, R., and Wang, Y. China's future generation. Assessing the maximum potential for renewable power sources in China to 2050. The World Wildlife Fund, Beijing (2014).
55. Standardization Administration of the People's Republic of China. GB 20052-2024 Minimum allowable values of energy efficiency and the energy efficiency grades for power transformers. (2024).
56. Parra, D., Valverde, L., Pino, F. J. & Patel, M. K. A review on the role, cost and value of hydrogen energy systems for deep decarbonisation. *Renew. Sustain. Energy Rev.* **101**, 279–294 (2019).
57. Parra, D. & Patel, M. K. Techno-economic implications of the electrolyser technology and size for power-to-gas systems. *Int. J. Hydrog. Energy* **41**, 3748–3761 (2016).
58. Hassan, A., Patel, M. K. & Parra, D. An assessment of the impacts of renewable and conventional electricity supply on the cost and value of power-to-gas. *Int. J. Hydrog. Energy* **44**, 9577–9593 (2019).
59. Ren, L. et al. Techno-economic feasibility study on HTS power cables. *IEEE Trans. Appl. Supercond.* **19**, 1774–1777 (2009).
60. Demir, M. E. & Dincer, I. Cost assessment and evaluation of various hydrogen delivery scenarios. *Int. J. Hydrog. Energy* **43**, 10420–10430 (2018).
61. Yu, Q., Hao, Y., Ali, K., Hua, Q. & Sun, L. Techno-economic analysis of hydrogen pipeline network in China based on levelized cost of transportation. *Energy Convers. Manag.* **301**, 118025 (2024).
62. Kim, S. H. et al. Electrical insulation characteristics of PPLP as a HTS DC cable dielectric and GFRP as insulating material for terminations. *IEEE Trans. Appl. Supercond.* **22**, 7700104 (2011).
63. Amaral, P. C. S., Oh, C. B., Do, K. H. & Choi, B. I. Risk assessment of hydrogen leakage and explosion in a liquid hydrogen facility using computational analysis. *Int. J. Hydrog. Energy* **91**, 950–964 (2024).
64. Verfondern, K. et al. Handbook of hydrogen safety: Chapter on LH2 safety. *Pre-normative REsearch for Safe use of Liquid Hydrogen (PRESLHY)*. https://hysafe.info/wp-content/uploads/sites/3/2021/04/D39_2021-01-PRESLHY_ChapterLH2-v3.pdf (2021).
65. Weidner, T., Tulus, V. & Guillén-Gosálbez, G. Environmental sustainability assessment of large-scale hydrogen production using prospective life cycle analysis. *Int. J. Hydrog. energy* **48**, 8310–8327 (2023).
66. Kim, J. H., Park, D. K., Kim, T. J. & Seo, J. K. Thermal-structural characteristics of multi-layer vacuum-insulated pipe for the transfer of cryogenic liquid hydrogen. *Metals* **12**, 549 (2022).
67. Wehr, M., Wolf, M. J. & Arndt, T. Experimental studies on indirect cooling for a hybrid power transfer line (LH_2 and HTS). *Cryogenics* **152**, 104206 (2025).
68. Qiu, Q. et al. General design of±100 kV/1kA energy pipeline for electric power and LNG transportation. *Cryogenics* **109**, 103120 (2020).
69. Zhang, C. et al. Review of offshore superconducting wind power generation for hydrogen production. *Energies* **18**, 1889 (2025).
70. Mukwanje, C. A., Faik, A. & Nachtane, M. Current progress, challenges, and future prospects in composite cryogenic hydrogen storage tanks. *Polym. Compos.* **46**, S48–S70 (2025).
71. Larbalestier, D., Gurevich, A., Feldmann, D. M. & Polyanskii, A. High-T_c superconducting materials for electric power applications. *Nature* **414**, 368–377 (2001).
72. Yao, C. & Ma, Y. Superconducting materials: Challenges and opportunities for large-scale applications. *Iscience* **24**, 102541 (2021).
73. Gömöry, F. & Klinčok, B. Self-field critical current of a conductor with an elliptical cross-section. *Supercond. Sci. Technol.* **19**, 732 (2006).
74. Grilli, F. et al. Numerical modeling of MgB_2 conductors for high power AC transmission. *Phys. C Supercond. Appl.* **504**, 167–171 (2014).
75. Klöppel, S., Marian, A., Haberstroh, C. & Bruzek, C. E. Thermo-hydraulic and economic aspects of long-length high-power MgB_2 superconducting cables. *Cryogenics* **113**, 103211 (2021).
76. Wang, Y. *Fundamental Elements of Applied Superconductivity in Electrical Engineering* (John Wiley & Sons, 2013).
77. Morandi, A. HTS dc transmission and distribution: concepts, applications and benefits. *Supercond. Sci. Technol.* **28**, 123001 (2015).
78. Muzzi, L., De Marzi, G., Di Zenobio, A. & Della Corte, A. Cable-in-conduit conductors: lessons from the recent past for future developments with low and high temperature superconductors. *Supercond. Sci. Technol.* **28**, 053001 (2015).
79. Musso, A. et al. Techno-economic assessment of coaxial HTS HVAC transmission cables with critical current grading between phases using the OSCaR tool. *Appl. Sci.* **14**, 2076–3417 (2024).

80. Guerra, O. J., Eichman, J., Kurtz, J. & Hodge, B. M. Cost competitiveness of electrolytic hydrogen. *Joule* **3**, 2425–2443 (2019).
81. Chen, Q., Gu, Y., Tang, Z., Wang, D. & Wu, Q. Optimal design and techno-economic assessment of low-carbon hydrogen supply pathways for a refueling station located in Shanghai. *Energy* **237**, 121584 (2021).
82. Zhu, Z. et al. Technical and economic analysis on long-distance hydrogen pipeline transportation. *Pet. Sci. Bull.* **8**, 112–124 (2023).
83. Zhu, Z., Lu, S., Gao, B., Yi, T. & Chen, B. Life cycle cost analysis of three types of power lines in 10 kV distribution network. *Inventions* **1**, 20 (2016).
84. National Energy Administration (NEA). https://www.nea.gov.cn/pdf/0608nyj.pdf.
85. Yang, M., Hunger, R., Berrettoni, S., Sprecher, B. & Wang, B. A review of hydrogen storage and transport technologies. *Clean. Energy* **7**, 190–216 (2023).
86. Solomon, M. D., Heineken, W., Scheffler, M. & Birth-Reichert, T. Cost optimization of compressed hydrogen gas transport via trucks and pipelines. *Energy Technol.* **12**, 2300785 (2024).
87. Curcio, E. Techno-economic analysis of hydrogen production: Costs, policies, and scalability in the transition to net-zero. *Int. J. Hydrog. Energy* **128**, 473–487 (2025).

Acknowledgements

This work was supported in part by the National Natural Science Foundation of China under Grant Nos. 52472382 and 52407025, and the Fundamental Research Funds for the Central Universities.

Author contributions

X.C., Y.C. and B.S. conceived and designed the research. X.C., L.F. and B.S. developed the framework and formulated the theoretical model. X.C., Y.C. and B.S. carried out the data search. Y.C., S.J., M.Z., Z.C., C.Z. and S.B. carried out the design and simulations. X.C., Y.C., M.Z., J.Y., G.W., Y.Z., L.F. and S.B. analyzed the data. X.C., Y.C., S.J., M.Z., J.Y., L.F. and B.S. contributed to the discussions and writing of this article.

Competing interests

The authors declare no competing interests.

Additional information

Supplementary information The online version contains supplementary material available at https://doi.org/10.1038/s44458-026-00077-z.

Correspondence and requests for materials should be addressed to Lin Fu or Boyang Shen.

Peer review information *Communications Sustainability* thanks Hanaa Feleafel and the other, anonymous, reviewer(s) for their contribution to the peer review of this work. Primary Handling Editor: Nandita Basu. A peer review file is available.